AAS 14-322

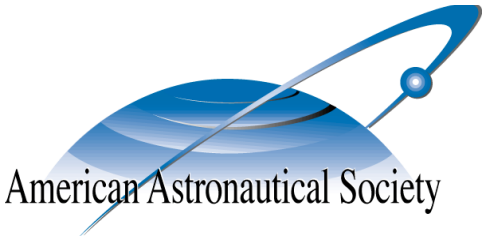

American Institute of
Aeronautics and Astronautics

CHARACTERIZING LOCALIZED DEBRIS CONGESTION IN THE GEOSYNCHRONOUS ORBIT REGIME

Paul V. Anderson and Hanspeter Schaub

AAS/AIAA Space Flight Mechanics Meeting

Santa Fe, NM **January 26 - 30, 2014**

AAS Publications Office, P.O. Box 28130, San Diego, CA 92198

AAS 14-322

CHARACTERIZING LOCALIZED DEBRIS CONGESTION IN THE GEOSYNCHRONOUS ORBIT REGIME

Paul V. Anderson* **and Hanspeter Schaub†**

Forecasting of localized debris congestion in the geostationary (GEO) ring is performed to investigate how frequently near-miss events occur for each of the GEO longitude slots on a daily basis, and characterize the classes of uncontrolled objects that contribute the most to macroscopic debris congestion, both globally and in a longitude-dependent sense. The present-day resident space object (RSO) population is propagated forward in time to assess congestion conditions over a 5-year time frame, and the "congestion culprits" are identified to yield recommendations for active debris removal initiatives that seek to clean-up particular longitude slots. Objects librating about one or both of the two gravitational wells located at 75°E and 105°W contribute 56% of the global congestion at GEO over a 5-year period, even though this object class constitutes 14% of the current GEO RSO population.

INTRODUCTION

The geostationary (GEO) regime is a unique commodity of the terrestrial satellite industry that is becoming increasingly contaminated with orbital debris,[1,2] but is heavily populated with high-value assets.[3] As the lack of atmospheric drag effects at the GEO altitude renders lifetimes of these debris essentially infinitely long, conjunction assessment must be performed to safeguard operational GEO satellites from potential collisions with the uncontrolled population. GEO satellites must maintain a specified longitude slot, and cannot simply phase shift to evade debris – therefore, analyses of the macroscopic behavior of the GEO debris population are required to describe debris fluxes through particular GEO longitude slots, and forecast how frequently operational assets in these regions must potentially perform maneuvers to mitigate conjunctions. Rather than presenting the high-precision analysis required with risk assessment and mitigation measures, this study builds upon the analysis of Reference 4, which illustrates a one-year, macroscopic congestion forecast for debris at GEO, to determine which localized regions of the GEO ring are, in general, most susceptible to rising levels of debris congestion. As overcrowding of this ring is growing into a serious concern for owners and operators internationally, knowledge of debris flux patterns—termed debris weather—is critical for space situational awareness operations at GEO. Of significant interest is determining which classes of uncontrolled objects contribute the most to congestion, both globally and locally, over a specified time frame. Assessing if subsets of the debris population contribute equally to congestion is critical information for active debris removal (ADR) initiatives seeking to "clean up" particular longitude slots for sustained utilization. Existing debris analysis tools[5,6] rely on inertially-fixed cells to detect debris cell passage events (CPE), such that results are often averaged over cell right ascension, and

*Graduate Research Assistant, Department of Aerospace Engineering Sciences, University of Colorado Boulder, 429 UCB, Boulder, CO, 80309.

†Professor, Department of Aerospace Engineering Sciences, University of Colorado Boulder, 429 UCB, Boulder, CO, 80309.

provided as a function of altitude and declination.[6] Following Reference 4, this study harnesses a toroidal cell configuration in the GEO ring to investigate the impact of various classes of large-scale, uncontrolled objects on GEO debris weather from a longitude-dependent perspective. Small-scale debris sources such as explosion and collision events, although considered recently in References 7-8, are not considered in this paper, nor are other growth mechanisms such as ejection of solid rocket motor (SRM) slag or shedding of multi-layered insulation (MLI).[9]

Using publicly-available U.S. Strategic Command tracking data and an orbit classification system established by the European Space Agency,[10] this paper will illustrate a 5-year debris forecast in the GEO ring for large-scale, trackable, and unclassified resident space objects (RSOs) with up-to-date two-line element (TLE) sets. The results of this 5-year debris simulation—which performs parallel propagation using 4×4 EGM-96 gravitation, luni-solar perturbations, and a nominal solar radiation pressure effect—will be used to characterize which classes of uncontrolled debris objects contribute the most to macroscopic debris weather from the standpoint of both global and longitude-dependent congestion. For ADR initiatives geared towards slot clean-up at particular longitudes, information such as that derived from debris simulations using the torus intersection metric is especially useful in helping to determine which classes of objects should be considered for removal in future attempts to alleviate longitude-dependent congestion, especially over high-impact and debris-critical regions such as the two gravitational wells at 75°E and 105°W.[4] The results of this work may thereby be harnessed in tandem with long-term debris prediction studies, such as that performed in Reference 11, to provide recommendations for architecture and design of potential ADR demonstration missions.

CURRENT RSO POPULATION AT GEO

The RSO population in the GEO ring is classified with a taxonomy used by the European Space Agency's DISCOS database (Database and Information System Characterising Objects in Space).[10] For GEO objects, seven orbit categories are selected to classify the type of orbits traversed by these objects. Table 1 gives a description of this classification system; note that only uncontrolled objects are assumed to contribute to local debris congestion in this study. GEO RSOs are selected according to the requirements imposed in the ESA *Classification of Geosynchronous Objects* reports:[10]

- Eccentricity smaller than 0.2 ($e < 0.2$)
- Inclination smaller than 70° ($i < 70^\circ$)
- Mean motion between 0.9 and 1.1 revolutions per sidereal day ($0.9 < n < 1.1$)*

Orbital data is obtained from the publicly-available two-line element (TLE) sets provided by U.S. Strategic Command (USSTRATCOM).† For this study, a reference TLE set obtained on 08/28/2013 is employed; the class distribution for the 1128 objects extracted from this set is shown in Figure 1. TLE data are provided in the form of doubly-averaged Keplerian elements with mean motion instead of semi-major axis,[6] transformed into Cartesian states within the true equator, mean equinox (TEME) frame[12] with SGP-4 theory.[13]‡ Note that because of the limited accuracy of TLE sets, these data are not intended for studies that require highly-precise orbit prediction capabilities. As the purpose of this paper is to forecast near-miss events occurring on a macroscopic, longitude-dependent

*This mean motion range corresponds to the semi-major axis range $[-2596, 3068]$ km with respect to the GEO radius.

†Publicly-available TLE data sets are available for bulk download from `https://www.space-track.org/`

‡ANSI-C implementation of merged SGP-4/SDP-4 theory is available from `http://www.sat.dundee.ac.uk/~psc/sgp4.html`[14]

Table 1. Orbit classifications for geosynchronous objects used in GEO congestion study.

Class	Type	Description
C1	Controlled	Longitude/inclination control (E-W/N-S control)
C2	Controlled	Longitude control only (E-W control only)
D	Drifting	Drift above/below/through protected GEO zone
L1	Librating	Libration about Eastern stable point ($\lambda = 75^{\circ}$E)
L2	Librating	Libration about Western stable point ($\lambda = 105^{\circ}$W)
L3	Librating	Libration about Eastern/Western stable points
IN	Indeterminate	Unknown status (e.g., recent TLE not available)

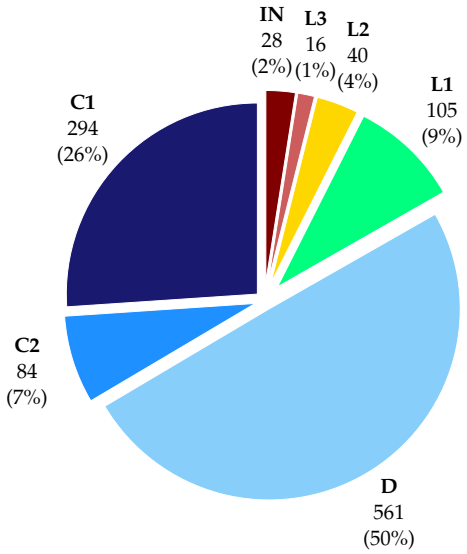

Figure 1. Orbit classifications for 08/28/13 reference TLE set.

scale, and evaluate the contributions of the orbit classes in Table 1 to local congestion, the accuracy of these data is sufficient.* Furthermore, as only objects larger than approximately 0.8-1.0 meter in effective diameter are actively tracked at the GEO altitude,[10] only objects at least of this size are considered. Since this study only incorporates the trackable, catalogued, and unclassified GEO RSOs with up-to-date TLEs, the findings of this study serve to illustrate a conservative lower bound of the actual debris congestion situation in the GEO ring, and present which classes of large-scale objects currently at GEO contribute the most to longitude-dependent congestion in this regime.

The Eastern librating (L1) and Western librating (L2) RSOs oscillate within the Earth-fixed frame around their respective gravitational wells with a libration period of 816 days at minimum for small amplitudes.[6] Using tabulated data in Reference 10, a histogram of the libration periods for the L1/L2 objects included in this study is provided in Figure 2. The mean of this libration period distribution is approximately 2.6 years, such that a 5-year time frame is used for this study to capture two mean cycles of the libration motion. In this manner, congestion results are kept as unbiased as possible.

*Numerical justification for using TLE data sets in a similar GEO debris congestion study is provided in Reference 11.

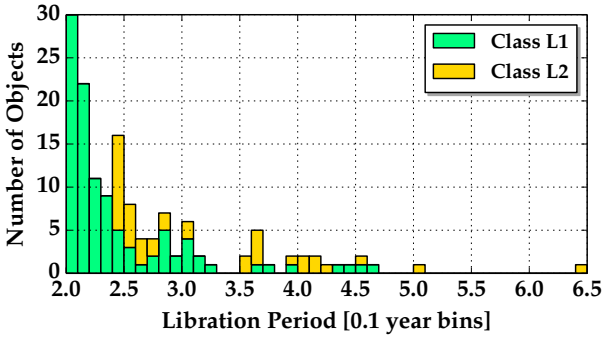

Figure 2. Libration periods for L1/L2 objects included in study.

FORECASTING LOCALIZED GEO CONGESTION

Overview of of Near-Miss Events Metric

The following metric for quantifying longitude-dependent debris congestion at GEO is discussed in detail in Reference 4, and summarized in this section for convenience. Near-miss events for the GEO longitude slots are determined by formulating a GEO-encompassing torus with major radius $r_{\text{GEO}} = 42164$ km and minor radius $\tilde{r}$, partitioned into longitude increments of $\Delta\lambda = 1.0^{\circ}$.[4] The minor radius $\tilde{r}$ is equivalent to the radius of the circular torus cross-section, and provides a means to evaluate debris congestion levels occurring within various distances of the GEO longitude slots – a larger minor radius captures more near-miss events. For this study, a representative minor radius of $\tilde{r} = 100$ km is considered, as this radius provides a rough upper bound for distances at which precise conjunction assessment could be considered for GEO satellites. Further, this torus formulation is a natural choice for evaluating CPE for the non-inertial GEO slots, as torus geometry is invariant as seen by both the inertial frame (i.e., MJ2000) and Earth-centered, Earth-fixed frame, in which these GEO longitude slots are fixed.[4]

Near-miss events are detected during propagation of an object by checking for the transversal of this GEO torus boundary at each time step during numerical integration; if finer resolution is desired, an interpolation scheme can implemented to check for torus intersections between integration time steps. Mathematically, a near-miss event occurs if[4]

$$\left(r_{\text{GEO}} - \sqrt{r_X^2 + r_Y^2}\right)^2 + r_Z^2 - \tilde{r}^2 < 0 \tag{1}$$

is satisfied, where $(r_X, r_Y, r_Z)^T$ is the RSO position vector expressed in inertial frame components. The longitude of intersection λ_{CPE} is thus determined as:

$$\lambda_{\text{CPE}} = \arctan\left(\frac{r_Y}{r_X}\right) - \alpha_G \tag{2}$$

where α_G is the right ascension of Greenwich (Greenwich sidereal time).[15] When a torus-intersection is detected with Equation (1), the longitude of intersection is determined with Equation (2), and the total near-miss count for the corresponding cell is updated. To ensure that equivalent intersections are not accounted for more than once during CPE checking, counting logic is used before a cell intersection counter is updated to screen the event for redundancy. The full algorithm for determining near-miss events with the GEO torus formulation is detailed in Reference 4.

Propagator and Implementation

A special perturbations propagation routine implemented in ANSI-C and parallelized with OpenCL is implemented to propagate the uncontrolled RSO population forward in time and determine torus intersection events.* A lower-fidelity, representative force model of the GEO environment is used for the added benefit of dramatically-decreased simulation run times. Here, the two-body equations of motion are numerically integrated under 4×4 EGM-96 gravitation, luni-solar perturbations, and solar radiation pressure (SRP), modeled with the cannonball assumption described in Reference 12, and attenuated with the occultation algorithm given in Reference 16. The equations of motion are

$$\ddot{\boldsymbol{r}} = -\frac{\mu_\oplus}{r^3}\boldsymbol{r} + \boldsymbol{a}_\oplus + \boldsymbol{a}_\leftmoon + \boldsymbol{a}_\odot + \boldsymbol{a}_{\text{SRP}} \tag{3}$$

where the first term denotes two-body acceleration, $\boldsymbol{a}_\oplus$ is the acceleration due to the nonsphericity of Earth, $\boldsymbol{a}_\leftmoon$ and $\boldsymbol{a}_\odot$ are the third-body perturbations from the Moon and Sun, respectively, and $\boldsymbol{a}_{\text{SRP}}$ is the SRP acceleration. SRP is modeled using the inverse-square diffusion formulation of the solar luminosity $L_\odot \approx 3.839 \times 10^{26}$ J/s, with coefficient of reflectivity $c_r \equiv 1.5$ and GEO-representative area-to-mass ratio $A_\odot/m = 0.04$ m^2/kg.† This GEO force model is in agreement with the results of Reference 8, which ranks the importance of incorporating various environmental perturbations in GEO force models for debris analysis over time scales ranging from 1 week to 10 years (the current study will consider macroscopic congestion over a 5-year period, a time scale over which luni-solar perturbations are especially relevant).

In higher-fidelity force models, coordinate transformations between Earth-fixed and Earth-inertial frames utilize accurate Earth orientation parameters to account for precession, nutation, and polar motion; software suites such as the SPICE toolkit can be harnessed to perform these complex coordinate transformations.‡ In this parallelized propagator, however, a lower-fidelity transformation that accounts strictly for a z-axis rotation by Greenwich sidereal time is used for purposes of increased speed at run time. Furthermore, instead of extracting inertial Moon and Sun position vectors from the DE-421 ephemerides, this routine implements low-precision formulae for the geocentric coordinates of these bodies, as provided in the 2013 *Astronomical Almanac*.[18] Reference 11 validates this lower-fidelity force model by comparing simulation results over a 5-year period with those obtained using a higher-fidelity force model. Since debris congestion results equivalent to those presented in the current paper change insignificantly when higher-fidelity forcing is used, lower-fidelity, parallel propagation is harnessed for the dramatic speed increase it provides.

The propagator utilizes an eighth-order, predictor-corrector Gauss-Jackson integrator[19] initialized with the Prince-Dormand 8(7) algorithm for integration of the equations of motion in Equation (3). During initial propagation of the uncontrolled RSO population to the CPE start date, and throughout near-miss computations in the prediction span, a 10 min time step is specified for sufficient fidelity in capturing macroscopic congestion trends. To enhance resolution without significantly increasing run times, linear interpolation is used to check for torus intersections in 1 min increments between primary time steps. Linear interpolation is an appropriate assumption in this case, because an object in a two-body GEO orbit will move through a circular arc of about $\theta_{\text{arc}} \approx 2.5^\circ$ in 10 minutes, such

*The *OpenCL 1.2 Specification* is available from Khronos Group at: `http://www.khronos.org/registry/cl/`.

†Reference 17 indicate that this ratio is representative for operational and defunct satellites at GEO; this value is thus used in the SRP computation for all RSOs considered in this study.

‡Jet Propulsion Laboratory's SPICE toolkits are available at `http://naif.jpl.nasa.gov/naif/toolkit.html`.

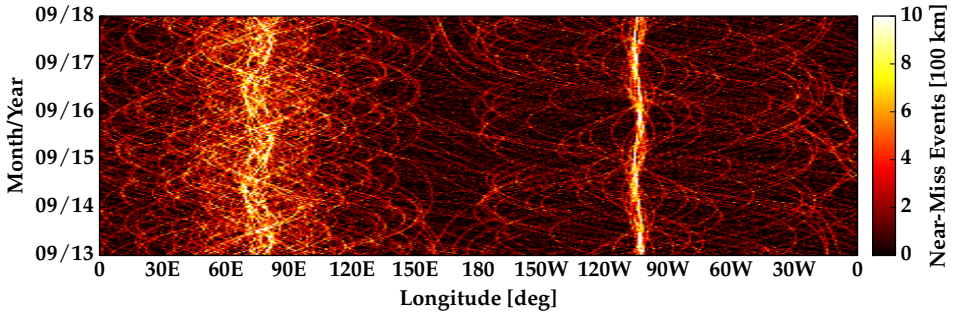

(a) Near-miss events per day at 100 km for 5-year GEO congestion forecasting period.

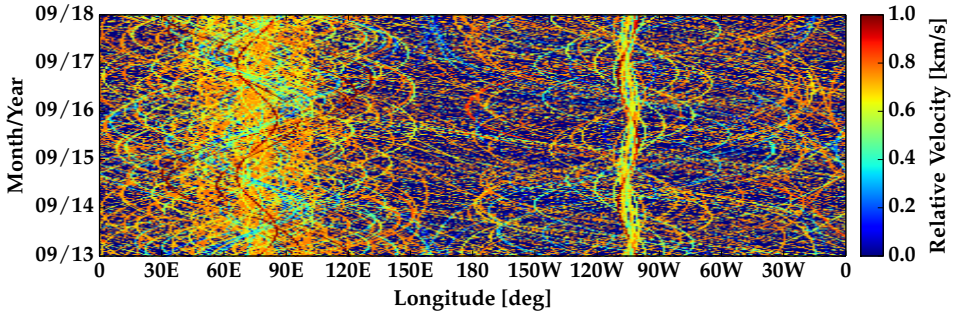

(b) Average relative velocity of near-miss events during 5-year congestion forecasting period.

Figure 3. Five-year localized debris congestion forecast at GEO, using 08/28/2013 TLE set.

that at the GEO altitude, the straight-line approximation over this time span will only deviate from the true curvilinear orbit by approximately $r_{\text{GEO}}\left[1-\cos(\theta_{\text{arc}}/2)\right] \approx 10$ km at maximum, based on the geometry of circular segments. Since the GEO torus considered here has a minor radius of 100 km, this discrepancy does not present a significant issue for this study.

Results of Debris Weather Forecast

As a precursor to identifying which classes of objects contribute the most to longitude-dependent debris weather in this regime, a 5-year macroscopic congestion forecast is performed with the minor radius $\tilde{r} = 100$ km, using the baseline RSO population in the 08/28/2013 TLE set. Controlled assets (C1/C2) are assumed to maintain their specified longitude slots, while the 750 uncontrolled objects extracted from this set are propagated forward in time and incorporated in the near-miss study. Note that this simulation is only assessing the congestion generated by the current debris population over a 5-year time frame. Nominal population growth,* fragmentation events, solid rocket motor (SRM) slag, multi-layered insulation (MLI) shedding, and other debris growth mechanisms considered in Reference 9, for example, are not treated in this simulation. Again, the objective of this paper is to investigate which classes of uncontrolled debris *currently* at GEO contribute the most to longitude-dependent congestion, and assess whether subsets of this population are more "guilty" than others.

The debris weather forecast at GEO for the 5-year analysis period is shown in Figure 3(a), which illustrates the number of near-miss events *per day* at 100 km for each of the longitude slots at GEO.

*The effect of nominal launch traffic on longitude-dependent congestion at GEO is simulated in Reference 11.

Accumulation of uncontrolled objects around the gravitational wells at 75°E and 105°W is a well-known result, as is discussed by References 20-21, for example. This is a particularly troublesome notion, as operational GEO assets are typically inserted into longitude slots near these debris-critical longitudes,[11] and the probability of collision in the vicinity of these gravitational wells is seven times larger than in surrounding regions at GEO.[3,22] From Figure 3(a), controlled assets in the longitude slots neighboring the gravitational wells are subject to 6-10 "close calls" per day at a miss distance of 100 km – this is on-par with the factor of seven increase over the less congested longitudes (e.g., Atlantic/Pacific Oceans), which experience a maximum of 1-2 near-misses per day at this distance.

It is interesting to highlight that although the number of near-miss events for a particular longitude slot may be relatively benign on a daily basis, the relative velocity with which the near-misses occur may not be. Figure 3(b) illustrates mean relative velocities as compared with a two-body GEO orbit in each longitude slot, averaged over the relative intersection velocities of all RSOs that intersected a particular cell on each day. The relative velocity map dictates that even though a particular longitude slot may experience 1-2 near miss events per day, the average relative speed could be upwards of 0.6 km/s (approximately 1340 MPH*). In general, higher relative velocity averages can be attributed to uncontrolled RSOs with larger orbital inclinations, such that relative velocities at the ascending and descending nodes are increased with respect to the equatorial GEO orbit velocity. Using the law of cosines, the relative speed at which an inclined RSO approaches an equatorial GEO satellite is

$$v_{\text{rel}} = \sqrt{v_{\text{GEO}}^2 + v_{\text{RSO}}^2 - 2v_{\text{GEO}}v_{\text{RSO}}\cos\left(i_{\text{RSO}}\right)} \tag{4}$$

where v_{GEO} and v_{RSO} are the velocities of the GEO satellite and uncontrolled RSO in their respective two-body orbits, and i_{RSO} is the inclination of the uncontrolled RSO. Therefore, assuming that both objects are in circular orbits of radius r_{GEO}, such that $v_{\text{GEO}} = v_{\text{RSO}} = \sqrt{\mu_\oplus / r_{\text{GEO}}}$, the speed v_{rel} is

$$v_{\text{rel}} = v_{\text{GEO}}\sqrt{2\left[1 - \cos\left(i_{\text{RSO}}\right)\right]} \implies 0 \leqslant v_{\text{rel}} \leqslant \sqrt{2}v_{\text{GEO}} \tag{5}$$

Since only RSOs satisfying $i_{\text{RSO}} < 70^\circ$ are considered for this study, a maximum relative velocity of $v_{\text{rel,max}} \approx 3.53$ km/s can be observed under this circular orbit assumption. The objects extracted from the TLE sets have nonzero eccentricity, however – Figure 4 shows the influence of eccentricity on the penetration of the 100 km GEO torus. Each vertical line illustrates the relative altitude range an RSO travels through during one revolution, as a function of semi-major axis deviation from the GEO radius, and each line is furthermore colored by the inclination of the RSO with respect to the equatorial plane. Upon brief inspection of this diagram, several threatening objects become immediately apparent, shown in this diagram as long, red lines, corresponding to high eccentricity and high inclination, respectively. These characteristic traits serve to increase relative velocities at the orbital nodes, rendering near-miss events with these particular RSOs more hazardous to operational assets.

IDENTIFYING CONGESTION CULPRITS

Global Congestion Culprits

To begin identifying the classes of uncontrolled debris objects in the GEO regime that contribute the most to longitude-dependent congestion, the results of the near-miss study simulation in Figure 3

*Relative velocities are lower in the GEO regime when compared to the LEO regime, since (a) orbit velocity is lower at the GEO altitude, and (b) objects at GEO are in general orbiting in the same direction.[8] Compared to the 2009 Iridium-33/Cosmos-2251 collision, which occurred at a relative speed of approximately 22,300 MPH (10 km/s), 1340 MPH is a benign, but still mission-ending collision velocity, particularly if the debris object involved is large/massive (rocket body).

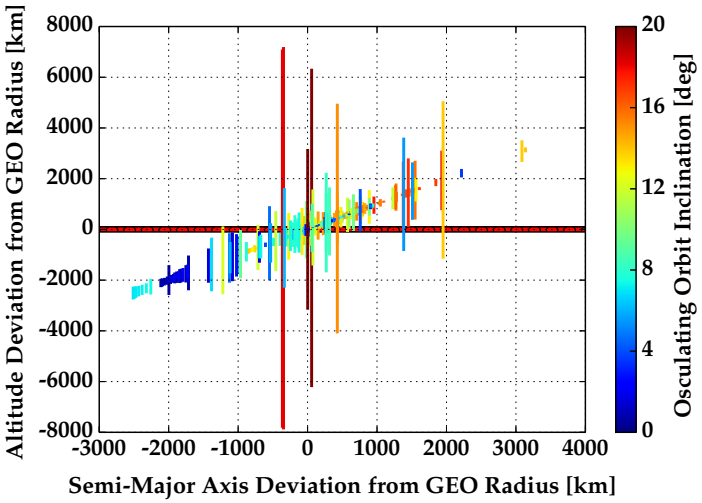

Figure 4. Effect of eccentricity on penetration of 100 km torus.

are partitioned by orbit type. Figure 5(a) gives a breakdown of the percentage that each uncontrolled orbit class contributed to the total number of near-miss events at 100 km occurring globally over the entire 5-year analysis period. This pie chart is interesting when compared alongside the TLE orbit class breakdown in Figure 1. Although drifting objects constitute 50% of the large-scale, trackable RSO population at GEO, they only contribute 34% of the near-miss events in this period. Librating objects, on the other hand, contribute a dominating 56% to the number of near-misses, even though these objects collectively make up a mere 14% of the RSO population at GEO. Similarly, the 28 IN objects simulated for this study (2% of the population) contribute 7% to the number of near-misses. Of significant interest for ADR initiatives are the 105 Eastern librating (L1) objects that contribute 37% to the number of near-misses. Without even considering *where* these near-miss events occur in a longitude-dependent sense, it is evident that these 105 objects are the most "guilty" of macroscopic congestion from this preliminary near-miss event breakdown.

Although Figure 5(a) gives a congestion breakdown by orbit class, it does not illustrate how much is contributed by individual RSOs within each orbit class – that is, of the 105 L1 objects, did a subset of this class contribute the entirety of the 37%, or did *all* L1 objects contribute homogeneously to this overall class contribution? Figures 5(b)-5(f) illustrate histograms for the individual percentage contributed to each overall orbit class percentage given in Figure 5(a). As illustrated in Figure 5(b), nearly 400 of the 561 drifting objects contribute less than 0.1% of the number of class D near-misses; on the other hand, only 29 of the drifting objects contribute at least 1.0% of these near-misses. Thus, the drifting population is nonhomogeneous in that the majority of these objects contribute very little to the overall 34% class D congestion contribution. On inspection of Figures 5(c)-5(e), we find that the librating object populations exhibit more homogeneity in that large majorities of each population contribute equivalently to the class L1/L2/L3 near-miss counts. Studying Figure 5(c), for example, we find that 88 of the 105 L1 objects contribute 0.9-1.0% of the overall 37% class L1 near-misses, such that each of these objects is equally "guilty" of contributing to macroscopic congestion at GEO in a global, longitude-independent sense. Results for the indeterminate class, shown in Figure 5(f), indicate that 18 of the 28 IN objects are responsible for at least 5% per object of the overall 7% class IN congestion contribution.

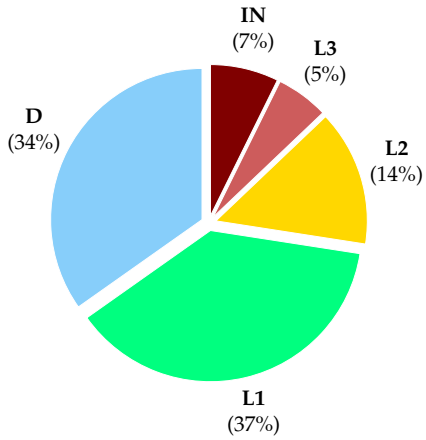

(a) 5-year near-miss breakdown by class.

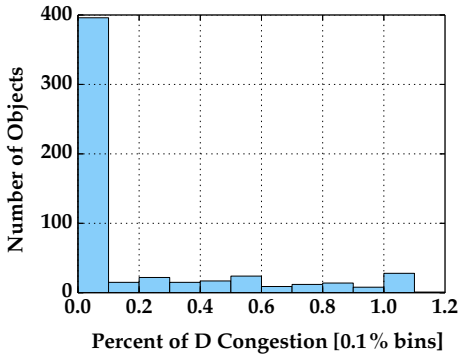

(b) Contribution to 34% class D congestion.

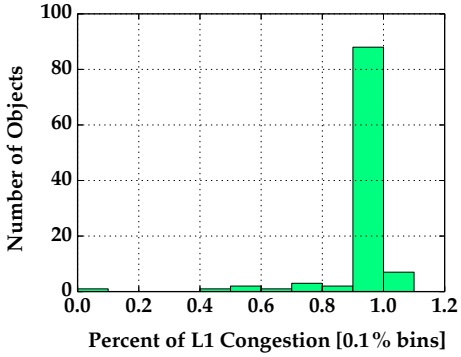

(c) Contribution to 37% class L1 congestion.

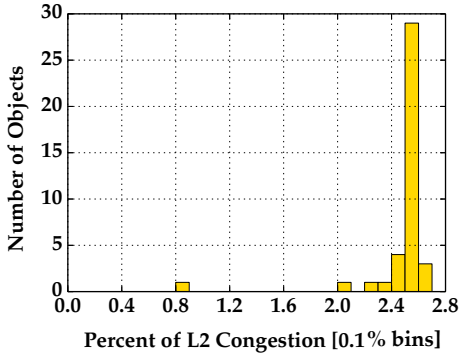

(d) Contribution to 14% class L2 congestion.

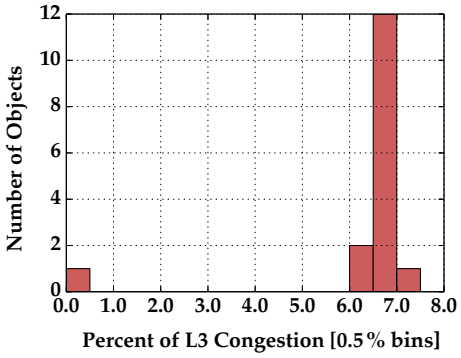

(e) Contribution to 5% class L3 congestion.

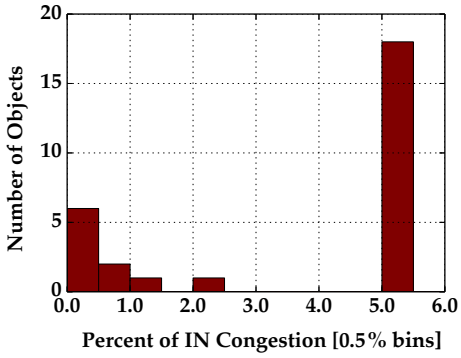

(f) Contribution to 7% class IN congestion.

Figure 5. Congestion distributions for near-miss events at 100 km tracked over 5-year period.

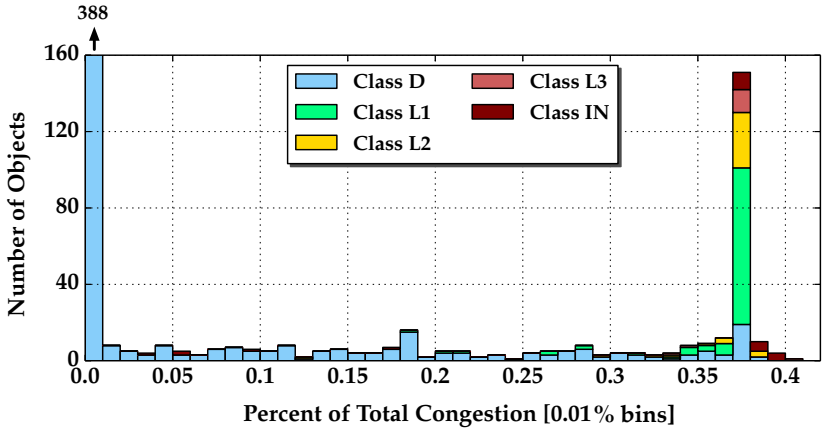

Figure 6. Contribution of individual RSOs to total near-miss events at 100 km over 5-year period.

To summarize, Figure 6 illustrates individual debris contributions to the total number of near-miss events at 100 km observed over this 5-year analysis period. From this chart, the global congestion culprits may be identified as all of the debris objects that contribute greater than 0.35% individually to the total number of near-miss events occurring during this time frame. From Figure 6, we observe that 29/561 D, 91/105 L1, 36/40 L2, 13/16 L3, and 18/28 IN objects satisfy this criterion. Based on this result, we conclude that the libration class objects—especially those of the Eastern librating type (L1)—are to blame for the majority of macroscopic congestion occurring globally around the GEO ring, that is, the class L objects contribute the majority of the near-miss events at 100 km occurring throughout GEO over this 5-year period. Therefore, from this perspective, ADR initiatives seeking to attenuate global congestion at GEO should seek to first consider the removal of this subset of the uncontrolled population. Although the results up to this point have identified the congestion culprits from a *global* perspective, it does not address which objects should be considered for removal if a particular longitude slot of interest is to be cleared of debris objects. Next, these 5-year simulation results are harnessed to identify macroscopic congestion culprits from a *longitude-dependent* basis.

Longitude-Dependent Congestion Culprits

In addition to tracking the number of near-misses at 100 km occurring daily for each longitude slot over this 5-year analysis period (cf. Figure 3), it is of interest to assess which classes of uncontrolled objects contribute the most to longitude-dependent congestion for purposes of recommending which types of objects to remove if a particular longitude slot is to be cleared of debris. Figure 7(a) shows the average number of near-miss events per day contributed by objects of each orbit class considered in this study. Longitude slots neighboring the debris-critical gravitational wells at 75°E and 105°W are subject to upwards of 6 close-calls per day, a factor of six increase over less congested longitude slots that experience only 1 close-call per day on average. As is anticipated, congestion contributions in the regions surrounding the Eastern and Western gravitation wells are dominated by the Eastern (L1) and Western (L2) librating objects, which oscillate in the Earth-fixed frame around these stable points with a libration period of 816 days at minimum for small amplitudes.[6] On average, the drift (D) objects contribute an approximate 0.5 near-misses per day across the entirety of the GEO ring, thereby generating the "background noise" observed in the debris congestion forecast in Figure 3(a). Increased contributions of the indeterminate (IN) class to slots around the gravitational wells suggest

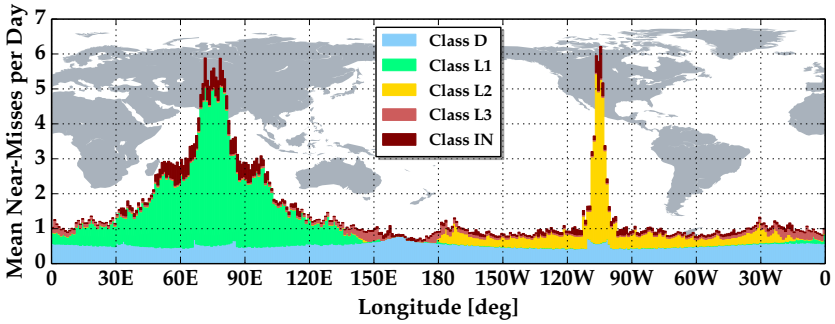

(a) Mean number of near-miss events per day at 100 km contributed by each orbit class.

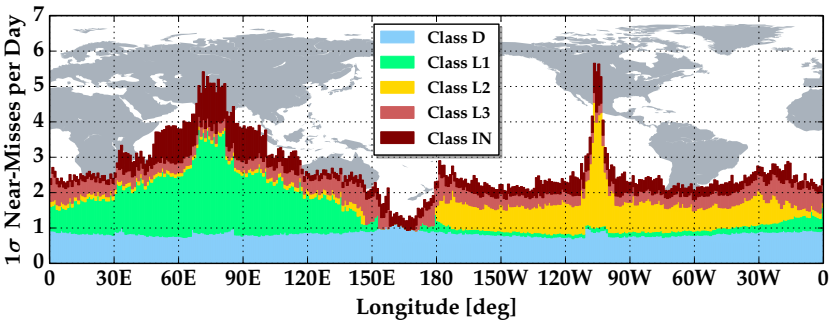

(b) Standard deviation (1σ) of near-miss events per day at 100 km for each orbit class.

Figure 7. Orbit class contributions to longitude-dependent congestion over 5-year period.

that a majority of these objects—likely those in the upper extreme of Figure 5(f)—are of the librating orbit classes. Studying Figure 7(a), it is evident that these L objects are congestion culprits from both the global and longitude-dependent perspectives. Reference 11 illustrates that operational assets are most frequently inserted into longitude slots in the vicinity of the debris-critical gravitational wells, making these L1/L2 objects ideal targets for ADR initiatives seeking to attenuate congestion in these popular and often-utilized longitude slots.

For purposes of slot safety assessment, it is useful to consider not only the mean of the number of near-misses occurring daily for every longitude slot, but the standard deviation for this distribution, as well. Figure 7(b) illustrates the 1σ contribution for each orbit class to the number of near-misses occurring in each slot, highlighting the spread of these near-miss distributions generated by tracking the number of orbit class contributions to each slot, on each day of the 5-year analysis period. Near-miss distributions for the librating objects around the two gravitational wells have a larger 1σ spread, indicating that these congested slots can experience many more near-misses in a given day than the 5-year average of approximately 4.5 misses per day. To illustrate this, Figure 8 provides histograms of the near-miss distributions for L1 objects at 75°E, and L2 objects at 105°W, the locations of the two gravitational wells. These histograms illustrate occurrences of analysis days in which upwards of 10 near-misses *per day* attributed to librating objects alone occurred for both of these longitude slots. Thus, Figure 8 serves to further emphasize that ADR efforts aimed at attenuating congestion in longitude slots surrounding these gravitational wells should first consider the removal of librating objects in mission design and architecture analyses. Note that "out-of-place" 1σ contributions of L1 objects around the Western well and L2 objects around the Eastern well are attributed to 3-4

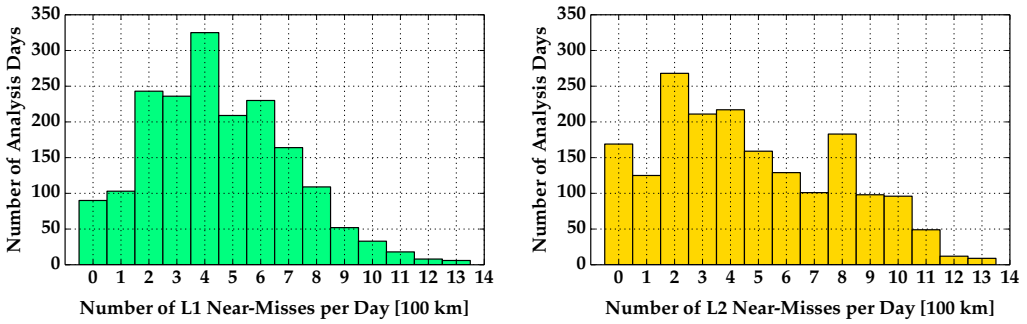

(a) L1 near-miss distribution for 75°E slot.

(b) L2 near-miss distribution for 105°W slot.

Figure 8. Near-miss distributions for L1/L2 objects over gravitational wells during 5-year period.

L1/L2 objects that—although identified as L1 or L2 in Reference 10—are now exhibiting L3 class behavior.

CONCLUSIONS

In this paper, forecasting of localized debris congestion in the GEO regime is performed to assess how many near-miss events at 100 km occur on a daily basis for each of the longitude slots at GEO over a 5-year analysis period. Utilizing a torus intersection metric in tandem with publicly-available TLE tracking data, the classes of objects that contribute the most to longitude-dependent congestion from both global and longitude-dependent perspectives are identified. Simulation results dictate that the librating class objects—especially those of the Eastern librating class—are the most to blame for both global and longitude-dependent congestion levels, especially for longitude slots surrounding the two debris-critical gravitational wells at GEO: 91 of the 105 L1 objects simulated for this study contribute greater than 0.35% individually to the total number of near-miss events observed globally during the 5-year analysis period, and these objects are responsible for 4.5 near-misses daily in the longitude slots surrounding the Eastern well at 75°E. Therefore, ADR initiatives seeking to globally reduce macroscopic congestion levels, or clean out particular longitude slots of interest, should first target the removal of L1/L2 librating class objects before considering the removal of drifting debris.

ACKNOWLEDGMENT

The authors would like to acknowledge the U.S. Department of Defense and the National Defense Science and Engineering Graduate Fellowship (NDSEG), the program through which funding for this research was obtained. The authors furthermore acknowledge Brandon Jones and the TurboProp software suite,[23] from which the integration routines employed in this research were obtained.

REFERENCES

[1] N. Johnson, "Protecting the GEO Environment: Policies and Practices," *Space Policy*, Vol. 15, 1999, pp. 127–135.

[2] R. Jehn, V. Agapov, and C. Hernandez, "The Situation in the Geostationary Ring," *Advances in Space Research*, Vol. 35, 2005, pp. 1318–1327.

[3] P. Chrystal, D. McKnight, and P. Meredith, "Space Debris: On Collision Course for Insurers?," tech. rep., Swiss Reinsurance Company Ltd, 2011.

[4] P. V. Anderson and H. Schaub, "Local Orbital Debris Flux Study in the Geostationary Ring," *Advances in Space Research*, Vol. 51, June 2013, pp. 2195–2206, http://dx.doi.org/10.1016/j.asr.2013.01.019.

[5] H. Lewis, G. Swinerd, N. Williams, and G. Gittins, "DAMAGE: A Dedicated GEO Debris Model Framework," *Proceedings of the Third European Conference on Space Debris*, Vol. 1, ESA Publications Division, March 2001.

[6] H. Klinkrad, *Space Debris: Models and Risk Analysis*. Praxis Publishing, 2006.

[7] D. Oltrogge and D. Finkleman, "Consequences of Debris Events in Geosynchronous Orbit," *Proceedings of the 2008 AIAA/AAS Astrodynamics Specialist Conference and Exhibit*, No. 2008-7375, August 2008.

[8] B. W. Hansen and M. E. Sorge, "Summarizing the General Effects of Breakup Debris in GEO," *Proceedings of the 2013 AAS/AIAA Astrodynamics Specialist Conference*, No. 13-844, August 2013.

[9] P. Wegener, J. Bendisch, H. Krag, M. Oswald, and S. Stabroth, "Population Evolution in the GEO Vicinity," *Advances in Space Research*, Vol. 34, 2004, pp. 1171–1176.

[10] T. Flohrer, "Classification of Geosynchronous Objects: Issue 15," Tech. Rep. 1, European Space Operations Centre, February 2013.

[11] P. V. Anderson and H. Schaub, "Local Debris Congestion in the Geosynchronous Environment with Population Augmentation," *Acta Astronautica*, Vol. 94, February 2014, pp. 619–628, http://dx.doi.org/10.1016/j.actaastro.2013.08.023.

[12] D. Vallado, *Fundamentals of Astrodynamics and Applications*. Microcosm Press, 3 ed., 2007.

[13] F. R. Hoots and R. L. Roehrich, "Spacetrack Report No. 3: Models for Propagation of NORAD Element Sets," tech. rep., Office of Astrodynamics, Aerospace Defense Center, December 1980.

[14] D. A. Vallado, P. Crawford, R. Hujsak, and T. S. Kelso, "Revisiting Spacetrack Report No. 3: Revision 2," *Proceedings of the 2006 AIAA/AAS Astrodynamics Specialist Conference*, August 2006.

[15] H. Curtis, *Orbital Mechanics for Engineering Students*. Elsevier Butterworth-Heinemann, 2005.

[16] O. Montenbruck and E. Gill, *Satellite Orbits: Models, Methods, Applications*. Springer, 2000.

[17] H. Schaub and L. E. Z. Jasper, "Circular Orbit Radius Control using Electrostatic Actuation for 2-Craft Configurations," *Proceedings of the 2011 AAS/AIAA Astrodynamics Specialist Conference*, August 2011.

[18] USNO and UKHO, *The Astronomical Almanac for the Year 2013*. U. S. Nautical Almanac Office with Her Majesty's Nautical Almanac Office, 2013.

[19] M. M. Berry and L. M. Healy, "Implementation of Gauss-Jackson Integration for Orbit Propagation," *Journal of the Astronautical Sciences*, Vol. 52, July-September 2004, pp. 331–357.

[20] K. Luu and C. Sabol, "Effects of Perturbations on Space Debris in Supersynchronous Storage Orbits," tech. rep., Air Force Research Laboratory, October 1998.

[21] V. A. Chobotov, ed., *Orbital Mechanics*. American Institute of Aeronautics and Astronautics, Inc., 3 ed., 2002.

[22] D. S. McKnight and F. R. Di Pentino, "New Insights on the Orbital Debris Collision Hazard at GEO," *Acta Astronautica*, Vol. 85, 2013, pp. 73–82.

[23] K. Hill and B. A. Jones, *TurboProp Version 4.0*. Colorado Center for Astrodynamics Research, University of Colorado at Boulder, May 2009.